SEMARAK ILMU PUBLISHING

Journal of Advanced Research in Fluid Mechanics and Thermal Sciences

Journal homepage:
https://semarakilmu.com.my/journals/index.php/fluid_mechanics_thermal_sciences/index
ISSN: 2289-7879

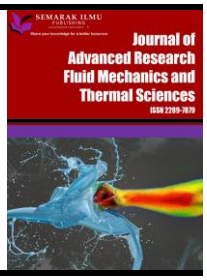

Radiative Blasius Hybrid Nanofluid Flow Over a Permeable Moving Surface with Convective Boundary Condition

Nur Syahirah Wahid[1,*], Nor Aliza Abd Rahmin[1], Norihan Md Arifin[1,2], Najiyah Safwa Khashi'ie[3], Ioan Pop[4,5], Norfifah Bachok[1,2], Mohd Ezad Hafidz Hafidzuddin[6]

[1] Department of Mathematics and Statistics, Faculty of Science Universiti Putra Malaysia, 43400 UPM Serdang, Selangor, Malaysia
[2] Institute for Mathematical Research, Universiti Putra Malaysia, 43400 UPM Serdang, Selangor, Malaysia
[3] Fakulti Teknologi Kejuruteraan Mekanikal dan Pembuatan, Universiti Teknikal Malaysia Melaka, Hang Tuah Jaya, 76100 Durian Tunggal, Melaka, Malaysia
[4] Department of Mathematics, Babeş-Bolyai University, R-400084 Cluj-Napoca, Romania
[5] Academy of Romanian Scientists, 3 Ilfov Street, 050044 Bucharest, Romania
[6] Centre of Foundation Studies for Agricultural Science, Universiti Putra Malaysia,43400 UPM Serdang, Selangor, Malaysia

ARTICLE INFO

Article history:
Received 23 May 2022
Received in revised form 10 October 2022
Accepted 21 October 2022
Available online 10 November 2022

Keywords:
Hybrid nanofluid; Blasius flow; suction; convective boundary condition; thermal radiation

ABSTRACT

The Blasius flow over a movable and permeable plate is envisaged in this study. Water-based hybrid nanofluid is incorporated with the insertion of thermal radiation, suction, and a convectively heated plate. The governing partial differential equations that simulate the fluid model are modified to ordinary differential equations through the implementation of self-similar transformation. A numerical solver known as bvp4c in Matlab is adopted to solve the problem numerically through the finite difference code with the Lobatto IIIa formula. Non-unique solutions are acquirable when the plate and the flow move in a dissimilar direction. As conducting the stability analysis, it is validated that the first solution is stable and reliable. The findings reveal that the imposition of stronger thermal radiation and greater Biot number for convection can lead to a better heat transfer performance. The 2% volume fraction of copper in the 1% volume fraction of alumina nanofluid composition would lead to greater skin friction when the plate is moving oppositely from the flow direction compared to the lesser volume fraction of copper. The boundary layer separation also can be efficiently prevented by composing a 2% copper volume fraction in the 1% alumina-water nanofluid compared to the lesser copper volume fraction.

1. Introduction

The flow of fluid across a fixed plate is a well-known phenomenon in fluid dynamics, especially in the context of the boundary layer. Blasius [1] is among the pioneer to investigate the boundary layer flow problem across an immovable semi-infinite flat plate while Sakiadis [2,3] is the first to study the flow across a movable plate. Since boundary layer flow and convective heat transfer problems can be significantly impacted by radiation at high operating temperatures, Bataller [4] extended the

* *Corresponding author.*
E-mail address: nursyahirahwahid95@yahoo.com

https://doi.org/10.37934/arfmts.100.3.115132

Blasius flow and heat transfer problem with the insertion of radiation effect and convective boundary condition over a flat plate [5]. A similar solution for radiative Blasius flow with a heated convective surface has also been reported by Aziz [6]. Later, Ishak *et al.,* [7] extended the radiative Blasius problem towards the movable plate instead of the static flat plate. Ahmad *et al.,* [8] then considered nanofluid towards the Blasius flow model. Following that, Bachok *et al.,* [9] examined the Blasius nanofluid flow past a movable plate. After several years, it seems that nanofluid has captivated the interest of researchers to envisage this kind of fluid especially by using the Blasius model.

After the development of the nanofluid by Choi and Eastman [10] as a new smart heat transfer fluid, a hybrid nanofluid then developed. It is the most recent type of heat transfer fluid with excellent potential for industrial applications due to the dispersion of hybridized nanoparticles in the basic fluid. This fluid is made up of metallic or non-metallic particles to form the proper combination of a hybrid nanofluid. The effectiveness of hybrid nanofluid in heat transportation is due to its synergistic impact when compared to single nanofluid [11]. Therefore, it is expected that hybrid nanofluid would have better thermal properties compared to single nanofluid and traditional fluid [12]. Recently, Berrehal *et al.,* [13] have investigated the hybrid nanofluid flow over a convectively moving wedge through the implementation of a mass-based model. They also conducted the entropy generation analysis. Sulochana and Kumar [14] presented the regression modeling of hybrid nanofluid flow with the heat generation and absorption effect. They stated that this effect has diminished the heat transfer in the hybrid nanofluid, but the higher concentration of nanoparticles could enhance the heat transfer progress. In the other work, they also investigated the hybrid nanofluid with different considerations of hybrid nanoparticles such as silver with molybdenum disulfide and single-walled carbon nanotubes with multi-walled carbon nanotubes [15,16]. In these models, the presence of hybrid nanoparticles with higher concentrations is also found to enhance the heat transfer progress of the fluid. See also the other literature regarding the flow of hybrid nanofluid by Dinarvand *et al.,* [17] and Wahid *et al.,* [18-22]. According to the literature, it seems various investigations have been conducted towards the hybrid nanofluid flow with various model configurations. However, there are still limited studies that focus their study on the implementation of the Blasius model. Several limited available studies on this topic, for example, are conducted by Olatundun and Makinde [23] with the consideration of convectively heated surfaces and different geometries of nanoparticles. Also, Khashi'ie *et al.,* [24] studied the viscous dissipative hybrid nanofluid flow with the adaptation of the Blasius model and report the dual solutions.

Motivated by the preceding studies, especially on hybrid nanofluid, the major goal of this study is to upgrade Blasius's pioneering work and extend the work by Ahmad *et al.,* [8], which is by implementing hybrid nanofluid flow in a combined effect of radiative and convective heated boundary condition over a moving plate to the classical Blasius flow problem. Hence, a brand-new Blasius mathematical model with the integration of a hybrid nanofluid is proposed. The MATLAB bvp4c built-in function that considers the finite difference code with the three-stage Lobatto IIIa formula is fully employed to solve the fluid flow problem and establish the mentioned goals. For validation purpose, several comparative solutions under a specific case have been generated, and a significant agreement on the solutions are achieved with the prior studies. The second goal of this study is to investigate the impact of specified physical parameters such as nanoparticle concentration, suction, thermal radiation, and Biot number on the hydrodynamic flow and heat transfer of a hybrid nanofluid. Thus, the flow control can be established through the considered parameters. The execution of dual solutions in this study also provides insight towards the flow separation control that is signified through the visibility of the critical point. Moreover, this study is not only just contributing to the finding of non-unique dual solutions, the third goal is to highlight the

stability feature holds by each of the solutions through the stability analysis. Hence, the reliability of the executed solutions is validated.

2. Mathematical Formulation

Consider the Blasius model for the water-based hybrid alumina-copper nanofluid flow with suction and Rosseland thermal radiation, as presentable in Figure 1, where (x, y)-axes are the Cartesian coordinates, and the flow occupies the domain $y \geq 0$, while u_w and u_e are the velocities of the moving plate and the free stream, respectively. The bottom surface of the plate is assumed to be heated by convection from a hot fluid at a temperature T_f which gives a heat transfer coefficient $\tilde{h}_f(x)$ and T_∞ is the temperature of the ambient. The suction or injection velocity at the boundary is v_w while the radiation heat flow q_r is provided via the Rosseland approximation.

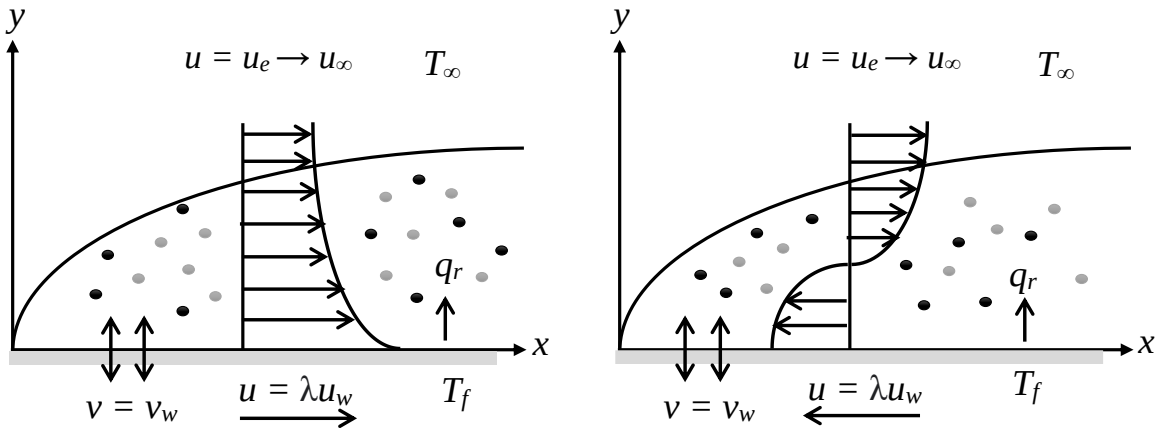

Fig. 1. Physical model illustration

The formulations for the Blasius hybrid nanofluid flow may be expressed as follows under the abovementioned assumptions [8,25]

$$\frac{\partial u}{\partial x} + \frac{\partial v}{\partial y} = 0, \tag{1}$$

$$u\frac{\partial u}{\partial x} + v\frac{\partial u}{\partial y} = \frac{\mu_{hnf}}{\rho_{hnf}}\frac{\partial^2 u}{\partial y^2}, \tag{2}$$

$$u\frac{\partial T}{\partial x} + v\frac{\partial T}{\partial y} = \frac{1}{\left(\rho C_p\right)_{hnf}}\left(k_{hnf}\frac{\partial^2 T}{\partial y^2} - \frac{\partial q_r}{\partial y}\right). \tag{3}$$

The boundary conditions are [6,24,26]

$$\begin{aligned} &u = u_w\lambda,\ v = v_w(x),\ -k_{hnf}\frac{\partial T}{\partial y} = \tilde{h}_f(x)\left(T_f - T\right) \text{ at } y = 0, \\ &u = u_e \to u_\infty,\ T \to T_\infty \text{ as } y \to \infty. \end{aligned} \tag{4}$$

Here, (u,v) are the velocity components of the hybrid nanofluid along (x,y)-axes, T is the temperature of the hybrid nanofluid, $\lambda<0$ indicates for the case when the plate moves oppositely from the flow direction (moves towards the slit), $\lambda>0$ indicates for the case when the plate moves in a similar direction with the flow (moves outwards the slit) and $\lambda=0$ is for the static plate where the problem reduces to those by Blasius. The dynamic viscosity, density, thermal conductivity and heat capacity of hybrid nanofluid is denoted by μ_{hnf}, ρ_{hnf}, k_{hnf} and $(\rho C_p)_{hnf}$ where the related relations are given in Table 1 [27,28].

Table 1
Thermophysical properties relations

Properties	Hybrid nanofluid
Density	$\rho_{hnf}=\phi_{Al_2O_3}\rho_{Al_2O_3}+\phi_{Cu}\rho_{Cu}+(1-\phi_{hnf})\rho_f$ where $\phi_{hnf}=\phi_{Al_2O_3}+\phi_{Cu}$
Heat capacity	$\left(\rho C_p\right)_{hnf}=\phi_{Al_2O_3}(\rho C_p)_{Al_2O_3}+\phi_{Cu}(\rho C_p)_{Cu}+\left(1-\phi_{hnf}\right)(\rho C_p)_f$
Dynamic viscosity	$\mu_{hnf}=\mu_f\left(1-\phi_{hnf}\right)^{-2.5}$
Thermal conductivity	$\frac{k_{hnf}}{k_f}=\left[\frac{\left(\frac{\phi_{Al_2O_3}k_{Al_2O_3}+\phi_{Cu}k_{Cu}}{\phi_{hnf}}\right)+2k_f+2\left(\phi_{Al_2O_3}k_{Al_2O_3}+\phi_{Cu}k_{Cu}\right)-2\phi_{hnf}k_f}{\left(\frac{\phi_{Al_2O_3}k_{Al_2O_3}+\phi_{Cu}k_{Cu}}{\phi_{hnf}}\right)+2k_f-\left(\phi_{Al_2O_3}k_{Al_2O_3}+\phi_{Cu}k_{Cu}\right)+\phi_{hnf}k_f}\right]$

Here, ϕ is the nanoparticle volume fraction ($\phi=0$ correspond to a classical fluid, $\phi_{Al_2O_3}\left(=\phi_1\right)$ corresponds to alumina and $\phi_{Cu}\left(=\phi_2\right)$ corresponds to copper). The subscript of f referring to the basic fluid which is water. The thermophysical properties of the composition in the hybrid nanofluid are given in Table 2 [29,30].

Table 2
Thermophysical properties for hybrid nanofluid

Properties	Water (f)	Alumina (Al_2O_3)	Copper (Cu)
$\rho\left(\mathrm{kg/m^3}\right)$	997.1	3970	8933
$C_p\left(\mathrm{J/kgK}\right)$	4179	765	385
$k\left(\mathrm{W/mK}\right)$	0.613	40	400
Pr	6.2	-	-

The radiative heat flux is commonly stated as below using the Rosseland [31] approximation [4,7]

$$q_r=-\frac{4\sigma^*}{3k^*}\frac{\partial T^4}{\partial y}, \tag{5}$$

where k^* and σ^* denote the coefficient of mean absorption and the constant of Stefan-Boltzmann, respectively. Implementing the Taylor series and neglecting higher-order terms, T^4 is expanded about T_∞ to get $T^4\approx 4T_\infty^3T-3T_\infty^4$. Hence, Eq. (3) is reformulated as

$$u\frac{\partial T}{\partial x}+v\frac{\partial T}{\partial y}=\frac{1}{\left(\rho C_p\right)_{hnf}}\left(k_{hnf}+\frac{16\sigma^* T_\infty^3}{3k^*}\right)\frac{\partial^2 T}{\partial y^2}. \tag{6}$$

It should be mentioned that in order that Eq. (1), Eq. (2), and Eq. (6) admit similarity solutions (reduce to ordinary differential equations), and presumably $\tilde{h}_f(x)=h_f x^{-1/2}$ where h_f is a constant.

Referencing Ahmad *et al.,* [8], the following similarity variables are proposed

$$u=u_{ref}f'(\eta),\ v=-\frac{1}{2}\sqrt{\frac{u_{ref}v_f}{x}}\left[f(\eta)-\eta f'(\eta)\right],\ \theta(\eta)=\frac{T-T_\infty}{T_f-T_\infty},\ \eta=y\sqrt{\frac{u_{ref}}{xv_f}} \tag{7}$$

with the suction velocity as

$$v_w=-\frac{1}{2}\sqrt{\frac{u_{ref}v_f}{x}}S \tag{8}$$

where the primes designate the differentiation respect to η, u_{ref} is either u_e or u_w, and $S>0$ is the suction parameter.

Substituting Eq. (7) into Eq. (2) and Eq. (6), the ordinary (similarity) differential equations are derived as below,

$$\left(\frac{\mu_{hnf}/\mu_f}{\rho_{hnf}/\rho_f}\right)f'''+\frac{1}{2}ff''=0, \tag{9}$$

$$\frac{1}{\Pr}\frac{1}{\left(\rho C_p\right)_{hnf}/\left(\rho C_p\right)_f}\left(\frac{k_{hnf}}{k_f}+\frac{4}{3}Rd\right)\theta''+\frac{1}{2}f\theta'=0, \tag{10}$$

subject to the boundary condition

$$\begin{aligned}&f(0)=S,\ f'(0)=\lambda,\ -\frac{k_{hnf}}{k_f}\theta'(0)=Bi\left[1-\theta(0)\right]\\&f'(\eta)\to 1,\ \theta(\eta)\to 0 \text{ as } \eta\to\infty\end{aligned} \tag{11}$$

Here, $\Pr$ is the Prandtl number, Rd is the radiation parameter, Bi is the Biot number, which is defined as

$$\Pr=\frac{\left(v\rho C_p\right)_f}{k_f},\ Rd=\frac{4\sigma^* T_\infty^3}{k^* k_f},\ Bi=\frac{h_f}{k_f}\sqrt{\frac{v_f}{u_{ref}}}. \tag{12}$$

The skin friction coefficients C_f and the local Nusselt number Nu_x, are defined as

$$C_f = \frac{\mu_{hnf}}{\rho_f u_{ref}^2}\left(\frac{\partial u}{\partial y}\right)_{y=0},\ Nu_x = \frac{x k_{hnf}}{k_f\left(T_f - T_\infty\right)}\left(-\frac{\partial T}{\partial y}\right)_{y=0} + \frac{x}{k_f\left(T_f - T_\infty\right)}\left(q_r\right)_{y=0}. \tag{13}$$

Using Eq. (7) and Eq. (13), we get

$$\mathrm{Re}_x^{1/2} C_f = \frac{\mu_{hnf}}{\mu_f} f''(0),\ \mathrm{Re}_x^{-1/2} Nu_x = -\left(\frac{k_{hnf}}{k_f} + \frac{4}{3}Rd\right)\theta'(0), \tag{14}$$

where $\mathrm{Re}_x = u_{ref} x / \nu_f$ is the local Reynolds number.

3. Stability Analysis

Since dual solutions are obtainable, it is necessary to examine the stability properties of the solutions [32]. To analyze the stable/unstable nature, following Weidman *et al.,* [33], the new self-similar variables that are time dependable should be introduced, as follows

$$\begin{gathered} u = u_{ref}\frac{\partial f}{\partial \eta}(\eta,\tau),\ v = -\frac{1}{2}\sqrt{\frac{u_{ref}\nu_f}{x}}\left[f(\eta,\tau) - \eta\frac{\partial f}{\partial \eta}(\eta,\tau)\right],\ \theta(\eta,\tau) = \frac{T - T_\infty}{T_f - T_\infty}, \\ \eta = y\sqrt{\frac{u_{ref}}{x\nu_f}},\ \tau = \frac{u_{ref} t}{x}, \end{gathered} \tag{15}$$

where τ is the non-dimensional time variable with time t. Inserting Eq. (15) into the time-dependable form of Eq. (2) and Eq. (6), to obtain

$$\left(\frac{\mu_{hnf}/\mu_{hnf}}{\rho_{hnf}/\rho_f}\right)\frac{\partial^3 f}{\partial \eta^3} + \frac{1}{2} f\frac{\partial^2 f}{\partial \eta^2} - \frac{\partial^2 f}{\partial \eta \partial \tau} = 0, \tag{16}$$

$$\frac{1}{\left(\rho C_p\right)_{hnf}/\left(\rho C_p\right)_f}\left(\frac{k_{hnf}}{k_f} + \frac{4}{3}Rd\right)\frac{\partial^2 \theta}{\partial \eta^2} + \frac{1}{2} f\frac{\partial \theta}{\partial \eta} - \frac{\partial \theta}{\partial \tau} = 0, \tag{17}$$

subject to the boundary condition

$$\begin{gathered} f(0,\tau) = S,\ \frac{\partial f}{\partial \eta}(0,\tau) = \lambda,\ -\frac{k_{hnf}}{k_f}\frac{\partial \theta}{\partial \eta}(0,\tau) = Bi\left[1 - \theta(0,\tau)\right], \\ \frac{\partial f}{\partial \eta}(\eta,\tau) \to 1,\ \theta(\eta,\tau) \to 0 \text{ as } \eta \to \infty. \end{gathered} \tag{18}$$

To determine the stability solutions that fulfill the boundary value problem of Eq. (9) and Eq. (10), the following relations should be considered towards Eq. (16) and Eq. (17),

$$\left.\begin{aligned} f(\eta,\tau) &= f_0(\eta) + e^{-\gamma\tau} F(\eta,\tau) \\ \theta(\eta,\tau) &= \theta_0(\eta) + e^{-\gamma\tau} Q(\eta,\tau) \end{aligned}\right\} \tag{19}$$

where γ is the eigenvalue parameter, $F(\eta,\tau)$ and $Q(\eta,\tau)$ are the small relative to $f_0(\eta)$ and $\theta_0(\eta)$, respectively. Hence, finally, the subsequent linearized eigenvalue problem can be obtained,

$$\left(\frac{\mu_{hnf}/\mu_{hnf}}{\rho_{hnf}/\rho_f}\right)F''' + \frac{1}{2}\left(F''f_0 + Ff_0''\right) + \gamma F' = 0, \tag{20}$$

$$\frac{1}{\left(\rho C_p\right)_{hnf}/\left(\rho C_p\right)_f}\left(\frac{k_{hnf}}{k_f} + \frac{4}{3}Rd\right)Q'' + \frac{1}{2}\left(f_0 Q' + F\theta_0'\right) + \gamma Q = 0, \tag{21}$$

subject to

$$\begin{aligned} &F(0) = 0,\ F'(0) = 0,\ \frac{k_{hnf}}{k_f}Q'(0) = BiQ(0), \\ &F'(\eta) \to 0,\ Q(\eta) \to 0 \text{ as } \eta \to \infty. \end{aligned} \tag{22}$$

It should be noted the stability of the solutions is identified through the (smallest) eigenvalue parameter γ_1 such that $\gamma_1 < \gamma_2 < \gamma_3 \ldots < \gamma_n < \gamma_{n+1}$. If $\gamma_1 < 0$, there is a development of perturbance and the flow is unstable; but when $\gamma_1 > 0$, there is a decay of perturbance, the flow is stable. The eigenvalues can be executed by relaxing the far-field boundary condition either $F'(\eta)$ or $Q(\eta)$ [34]. Therefore, $F'(\eta)$ is chosen to be relaxed and restated with $F''(0) = 1$ while solving and computing the unknown γ_1 from Eq. (20) and Eq. (21) with Eq. (22) that obey the relaxation procedure.

4. Numerical Computation in Bvp4c

Numerical solutions for the present problem are obtained via bvp4c in MATLAB. The bvp4c function is a finite-difference code that consists of the Lobatto-IIIa formula. All the numerical solutions executed from the present problem are subjected to a zero-error tolerance 10^{-10} with the boundary layer thickness of $\eta_\infty = 15$. To execute the solution from the bvp4c solver, we should first modify the resulting similarity equations. We assume that

$$f = y(1),\ f' = y(2),\ f'' = y(3),\ \theta = y(4),\ \theta' = y(5).$$

From this assumption, we can rewrite Eq. (9) and Eq. (10) into the following form

$$f''' = \frac{1}{\left(\frac{\mu_{hnf}/\mu_f}{\rho_{hnf}/\rho_f}\right)}\left(-\frac{1}{2}y(1)y(3)\right),$$

$$\theta'' = \frac{1}{\frac{1}{\Pr}\frac{1}{\left(\rho C_p\right)_{hnf}/\left(\rho C_p\right)_f}\left(\frac{k_{hnf}}{k_f}+\frac{4}{3}Rd\right)}\left(-\frac{1}{2}y(1)y(5)\right),$$

and Eq. (11) is rewritten as

$$\left.\begin{array}{l} ya(1)-S, ya(2)-\lambda, -\frac{k_{hnf}}{k_f}ya(5)-Bi\left[1-ya(4)\right], \\ yb(2)-1, yb(4), \end{array}\right\}$$

where ya refers to the condition when $\eta = 0$ and yb refers to the condition when $\eta \to \infty$. To run the solver, the appropriate value of governing parameters and the initial guesses for the solutions should be first applied. Several trial-and-error processes need to be undergone before the best possible solution can be obtained. We consider the solution to be correct when the convergence criteria have been met without any appearance of error or warning sign from the command window of the solver. Otherwise, the solution might be incorrect or might have exceeded the critical point within the setup configuration of parameters.

The same equations modification is also taken for the stability analysis in executing the unknown eigenvalues via bvp4c. We let the following assumptions towards Eq. (20) to Eq. (22):

$$\begin{array}{l} F = y(1), F' = y(2), F'' = y(3), Q = y(4), Q' = y(5), \\ f_0 = s(1), f_0' = s(2), f_0'' = s(3), \theta_0 = s(4), \theta_0' = s(5), \end{array}$$

so that we can rewrite them in bvp4c as:

$$F''' = \frac{1}{\left(\frac{\mu_{hnf}/\mu_{hnf}}{\rho_{hnf}/\rho_f}\right)}\left(-\frac{1}{2}\left(y(3)s(1)+y(1)s(3)\right)-\gamma y(2)\right),$$

$$Q'' = \frac{1}{\frac{1}{\left(\rho C_p\right)_{hnf}/\left(\rho C_p\right)_f}\left(\frac{k_{hnf}}{k_f}+\frac{4}{3}Rd\right)}\left(-\frac{1}{2}\left(s(1)y(5)+y(1)s(5)\right)-\gamma y(4)\right),$$

subject to the boundary condition

$$\left.\begin{array}{l} ya(1), ya(2), \frac{k_{hnf}}{k_f}ya(5)-Biya(4), \\ yb(2), yb(4). \end{array}\right\}$$

5. Results and Discussion

In this study, the suspension of the nanofluid is initially composed of $\phi_{Al_2O_3}(=\phi_1)=1\%$ alumina and water (base fluid) at Prandtl number = 6.2. The 1% alumina-water nanofluid is then hybridized with 1-2% of copper to form a hybrid nanofluid. The impact of different values of parameters such as copper volume fraction $(1\% \le \phi_{Cu}(=\phi_2) \le 2\%)$, Biot number $(1 \le Bi \le 3)$, thermal radiation $(1 \le Rd \le 3)$, and suction $(2.5 \le S \le 2.7)$ towards the physical quantities and profiles are illustrated in graphical form. The selected values for the parameters are depending on the suitability of the problem to generate the possible numerical solutions that satisfy the boundary conditions. The same ranges of parameter values have also been used in previous works such as those by Ahmad *et al.,* [8], Khashi'ie *et al.,* [24], and Abd Rahman *et al.,* [35]. Before generating the solutions to the present Blasius problem, some numerical validations have been made to validate our model and the computation. The numerical solutions in some comparable limiting cases are seen to be consistent with those previous studies (see Table 3 to Table 5).

Table 3
$\mathrm{Re}_x^{1/2} C_f$ when $Bi \to \infty$, $Rd = S = 0$, $\lambda = 0$, $\mathrm{Pr} = 6.2$

ϕ	Alumina-water nanofluid			Copper-water nanofluid		
	Present	Ahmad *et al.,* [8]; Abd Rahman *et al.,* [35]	Olatundun and Makinde [23]	Present	Ahmad *et al.,* [8]; Abd Rahman *et al.,* [35]	Olatundun and Makinde [23]
0	0.332057329	0.3321	0.332057	0.332057329	0.3321	0.332057
0.01	0.341231239	0.3412	-	0.349380342	0.3494	-
0.02	0.350556311	0.3551	0.350557	0.366653509	0.3667	0.366656
0.1	0.431591766	0.4316	-	0.507634096	0.5076	-
0.2	0.554509652	0.5545	-	0.706563210	0.7066	-

Table 4
Comparison values of $-\theta'(0)$ when $\phi_1 = \phi_2 = 0$, $Rd = S = 0$, $\lambda = 0$

Bi	$\mathrm{Pr} = 0.72$		$\mathrm{Pr} = 10$	
	Present	Aziz [6]	Present	Aziz [6]
0.1	0.074724189	0.0747	0.087924767	0.0879
0.2	0.119295479	0.1193	0.156903116	0.1569
0.4	0.169994382	0.1700	0.258173794	0.2582
1	0.228177799	0.2282	0.421343616	0.4213
5	0.279130997	0.2791	0.635582528	0.6356

Table 5
$\mathrm{Re}_x^{1/2} C_f$ and $\mathrm{Re}_x^{-1/2} Nu_x$ when $\phi_1 = 0.01$, $S = 0$, $\mathrm{Pr} = 6.2$

λ	Rd	Bi	ϕ_2	$\mathrm{Re}_x^{1/2} C_f$		$\mathrm{Re}_x^{-1/2} Nu_x$	
				Present	Khashi'ie *et al.,* [24]	Present	Khashi'ie *et al.,* [24]
-0.35	0	∞	0.01	0.196748581	0.19675	0.054609367	0.05461
				(0.136388415)	(0.13639)	(0.011260451)	(0.01126)
-0.3				0.272411307	0.27241	0.188443822	0.18844
				(0.272411309)	(0.18844)	(0.000307473)	(0.00031)
-0.25				0.306696364	0.30670	0.289350994	0.28935
				(0.034670581)	(0.03467)	(0.000012193)	(0.00001)
-0.2				0.328562567	0.32856	0.376355830	0.37636
				(0.016940533)	(0.01695)	(0.000000274)	(0.00000)
-0.3	0.5			0.272411313	0.27241	0.347430528	0.34743
				(0.064826997)	(0.06483)	(0.006602849)	(0.00660)
	1			0.272411315	0.27241	0.496993656	0.49699
				(0.064826996)	(0.06483)	(0.026764421)	(0.02676)
	1.5			0.272411329	0.27241	0.638224033	0.63822
				(0.064826993)	(0.06483)	(0.060498007)	(0.06050)
	2			0.272411342	0.27241	0.772545663	0.77255
				(0.064826992)	(0.06483)	(0.104162068)	(0.10416)
		0.1		0.272411362	-	0.241537690	-
				(0.064826994)		(0.080346181)	
		0.5		0.272411358	-	0.536605759	-
				(0.064826993)		(0.098332598)	
		1		0.272411351	-	0.633314758	-
				(0.064826992)		(0.101163422)	
			0.015	0.279032480	-	0.639375658	-
				(0.066402654)		(0.066402654)	
			0.02	0.285652509	-	0.645094919	-
				(0.067978054)		(0.112545146)	

Note: ( ) denotes the second solution

The distributions of $\mathrm{Re}_x^{1/2} C_f$ and $\mathrm{Re}_x^{-1/2} Nu_x$ with λ for several selected values of $\phi_2 \left(= \phi_{Cu}\right)$ when $Rd = Bi = 1$, $S = 2.5$ are illustrated in Figure 2 and Figure 3. In the region when the plate is moving in a similar direction to the flow direction $(\lambda > 0)$, it can be observed that the distribution of $\mathrm{Re}_x^{1/2} C_f$ is declining as ϕ_2 is gradually elevated from 1% to 2%. Also, there is no second solution exists within this range. Differently, when the plate is moving to oppose the flow direction $(\lambda < 0)$, the first and second solutions are noticed to exist and the distribution of $\mathrm{Re}_x^{1/2} C_f$ is uplifting for both solutions when ϕ_2 is elevated. This kind of configuration with higher ϕ_2 is suitable to improve the skin friction of a system. Meanwhile, the distribution of $\mathrm{Re}_x^{-1/2} Nu_x$ is contemplated to diminish under this configuration when ϕ_2 is upsurged in both first and the second solutions, regardless the direction of the moving plate. The presence of the suction parameter also plays a role in related to the heat transfer process, such that, $\mathrm{Re}_x^{-1/2} Nu_x$ will be increased with the increment of ϕ_2 if zero suction is considered (see Table 5), which, the finding is totally opposite compared to the condition when suction is configured (see Figure 3). As the domain moves towards the negative value of λ, the critical point λ_c for each selected ϕ_2 is presentable (see Figure 2 and Figure 3). The gradual increment of ϕ_2 from 1% to 1.5% and to 2%, expands (in magnitude) the value of $|\lambda_c|$ from 2.2882 to 2.3201

and to 2.3508, respectively. This implies that the boundary layer separation process can be prevented effectively when 2% copper is chosen compared to $1\%-1.5\%$.

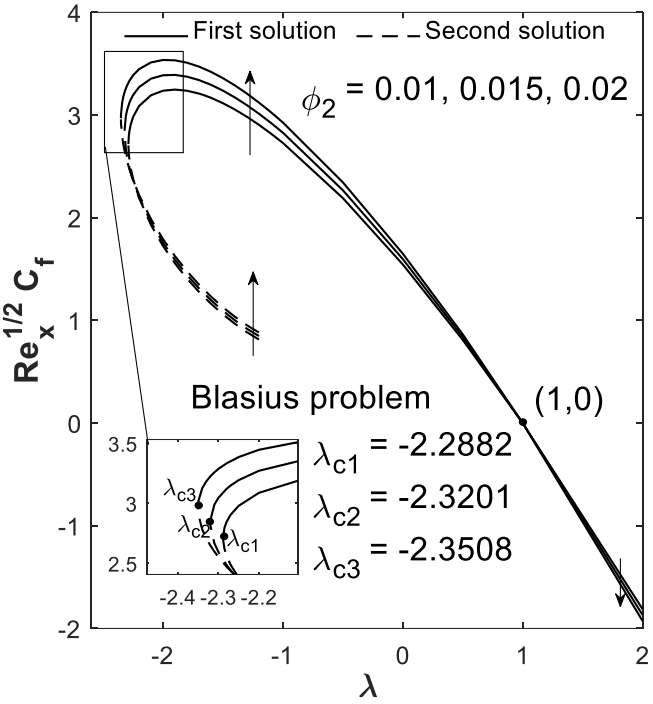

Fig. 2. $\mathrm{Re}_x^{1/2}\, C_f$ for selected ϕ_2

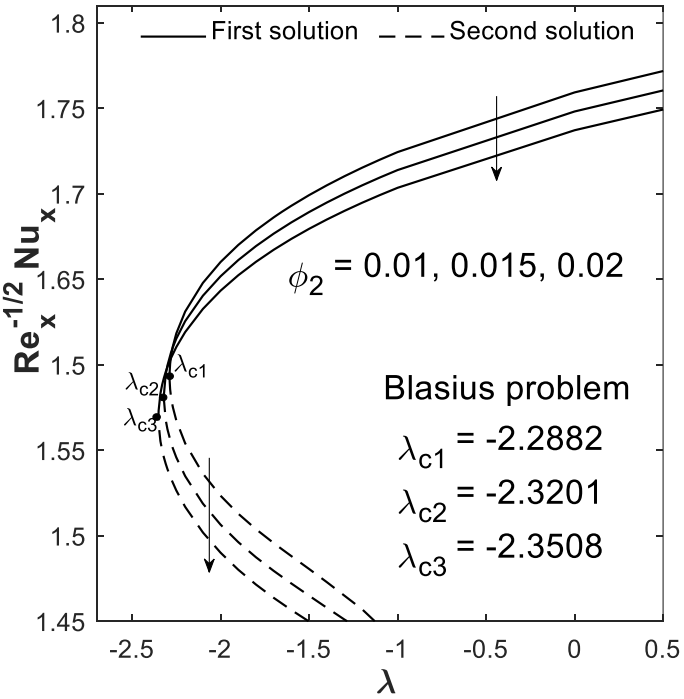

Fig. 3. $\mathrm{Re}_x^{-1/2}\, Nu_x$ for selected ϕ_2

Figure 4 and Figure 5 exhibit the distributions of $\mathrm{Re}_x^{-1/2}\, Nu_x$ with $-3 \le \lambda < 2$ for several selected values of Bi when $Rd = 1$, and for several values of Rd when $Bi = 1$, respectively, with $\phi_2\,(=\phi_{Cu}) = 1\%$ and $S = 2.5$. According to the figures, the surges of both Bi and Rd have improved

the value of $\mathrm{Re}_x^{-1/2} Nu_x$ for the first and the second solution. It is preferable to allow a larger value of these parameters to configure a cooling system. However, the second solution only appears when the plate is moving as opposed to the flow direction. The critical point too also exists at the negative region of λ but the changing in the values of Bi and Rd are not significant in this configuration/model to control the separation process of the boundary layer since the value of λ_c remains at the same point $(\lambda_c = -2.2882)$ for $Bi = Rd = 1, 2, 3$.

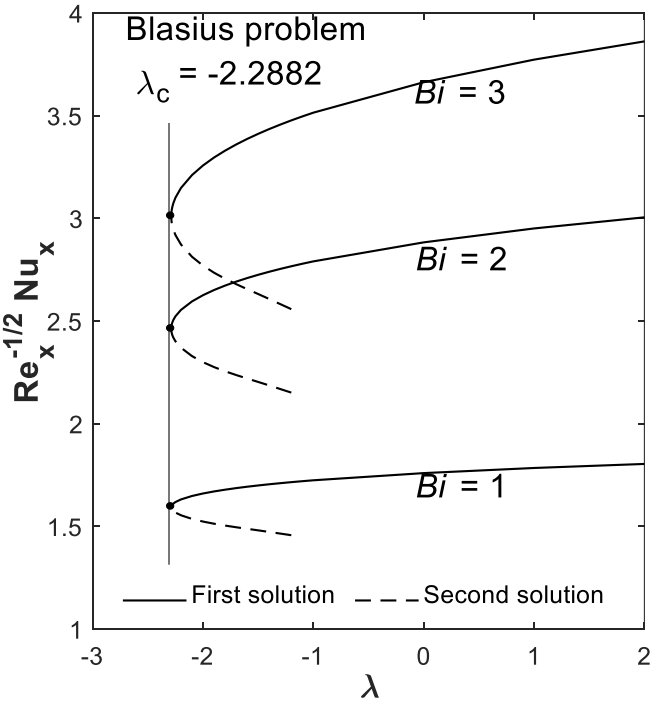

Fig. 4. $\mathrm{Re}_x^{-1/2} Nu_x$ for selected Bi

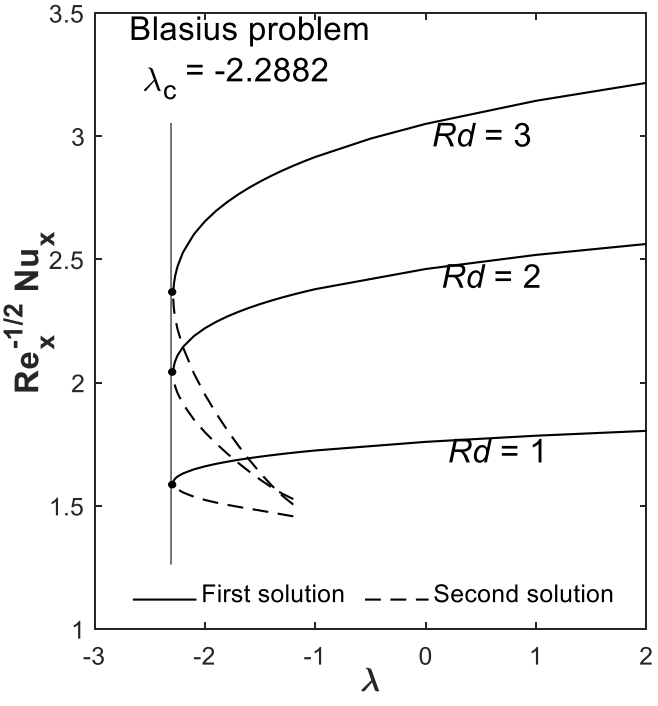

Fig. 5. $\mathrm{Re}_x^{-1/2} Nu_x$ for selected Rd

Figure 6 and Figure 7 portray the distributions of $\mathrm{Re}_x^{1/2} C_f$ and $\mathrm{Re}_x^{-1/2} Nu_x$ with λ for several selected values of S when $Rd = Bi = 1$, $\phi_2 \left(= \phi_{Cu}\right) = 1\%$. Within this parameter configuration, according to the first solution, the value of $\mathrm{Re}_x^{1/2} C_f$ is at the highest when stronger suction $S = 2.7$ is considered at the region when $\lambda < 0$, and is at the lowest when $S = 2.5$. However, when $\lambda > 0$, the result is inflected such that the inflection point is approximated to be located at the coordinate $(1,0)$. Zero $\mathrm{Re}_x^{1/2} C_f$ is noticed when $\lambda = 1$. Meanwhile, for the second solution, there also exists an inflection point that causes two different relations between S and $\mathrm{Re}_x^{1/2} C_f$, and the observed result is totally opposite to those of the first solution. The available numerical findings for the second solution are only procurable when $\lambda < 0$. Further, in the context of boundary layer separation, the critical point is seen to be expanded in magnitude when greater S is inserted, therefore this implies that a suitably stronger suction is recommended to inhibit the flow separation process and maintain the flow phase. The critical point for each different S is as the following: $\lambda_{c1} = -2.2882$ $(S = 2.5)$, $\lambda_{c2} = -2.4024$ $(S = 2.6)$, and $\lambda_{c3} = -2.5196$ $(S = 2.7)$. Additionally, the value of $\mathrm{Re}_x^{1/2} C_f$ is seen to be larger when $\lambda < 0$ compared to when $\lambda > 0$, meanwhile, the opposing observation is noticed towards the value of $\mathrm{Re}_x^{-1/2} Nu_x$ (see the first solution from Figure 2 to Figure 7). From a physical perspective, when $\lambda < 0$, the plate is moving in an opposing direction from the flow, therefore greater skin friction would be established compared to when the moving plate is moving in a similar direction with the flow. However, the heat transfer process occurs greatly when the plate moves outward from the slit that is assisted by the flow direction which causes the transfer of heat from the heated plate to easily occur.

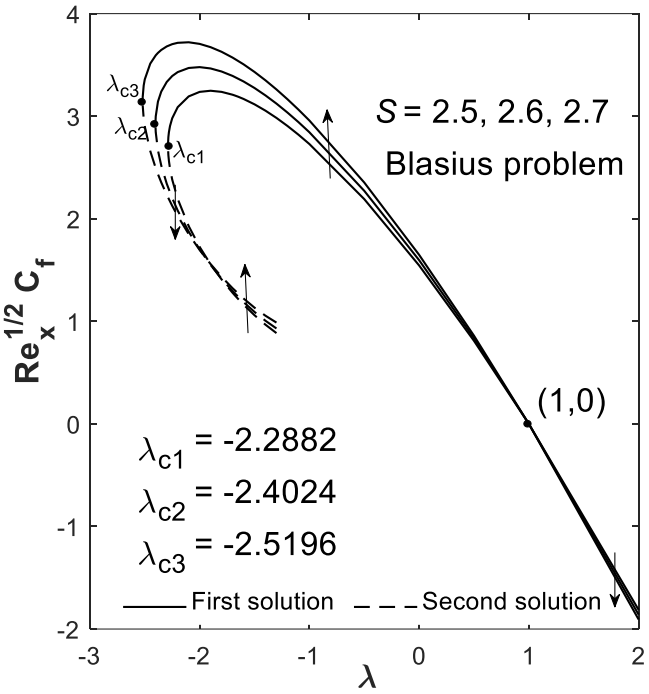

Fig. 6. $\mathrm{Re}_x^{1/2} C_f$ for selected S

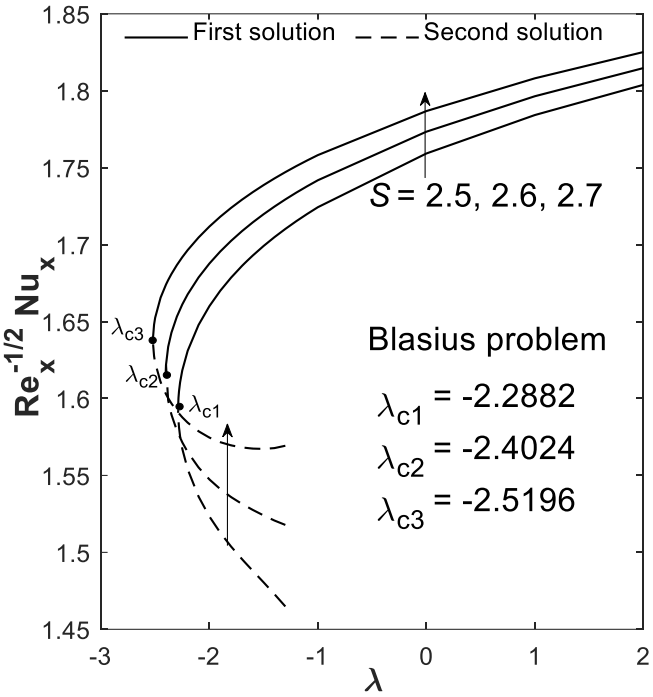

Fig. 7. $\mathrm{Re}_x^{-1/2}\ Nu_x$ for selected S

The profiles for the flow velocity and temperature are shown in Figure 8 and Figure 9 specifically for the case when the plate is moving in opposition to the flow direction. In this specific case, the boost of ϕ reacts oppositely towards the first and the second solution for each of the profiles. According to the first solution, the flow velocity is improvable when greater $\phi_2 (= 2\%)$ is considered, but contrarily for the second solution. Then again, a greater $\phi_2 (= 2\%)$ gives a lower temperature profile for the first solution compared to the other selected values, but conversely for the second solution. The thickness of the boundary layer for the first solution is also seen to be gradually thinned when enlarging the value of ϕ_2 towards the flow configuration, however, the contra behavior is given from the second solution.

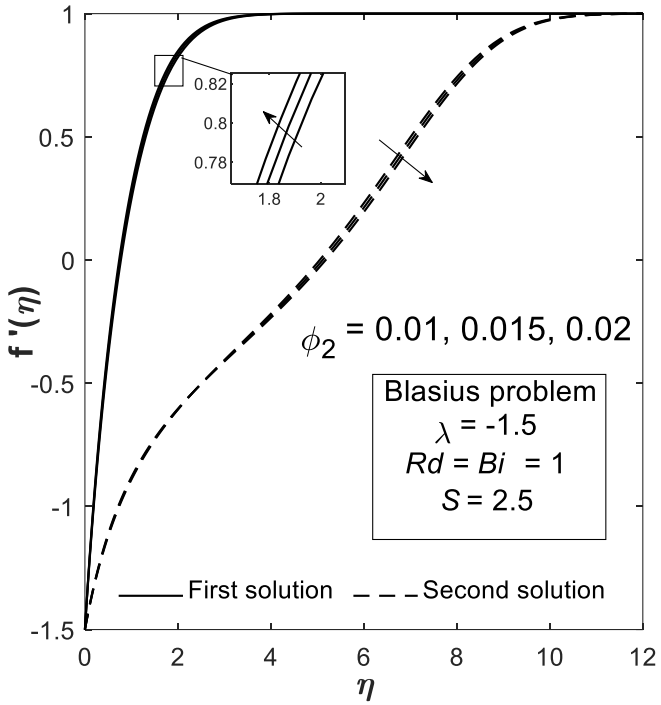

Fig. 8. Velocity profile for selected ϕ_2

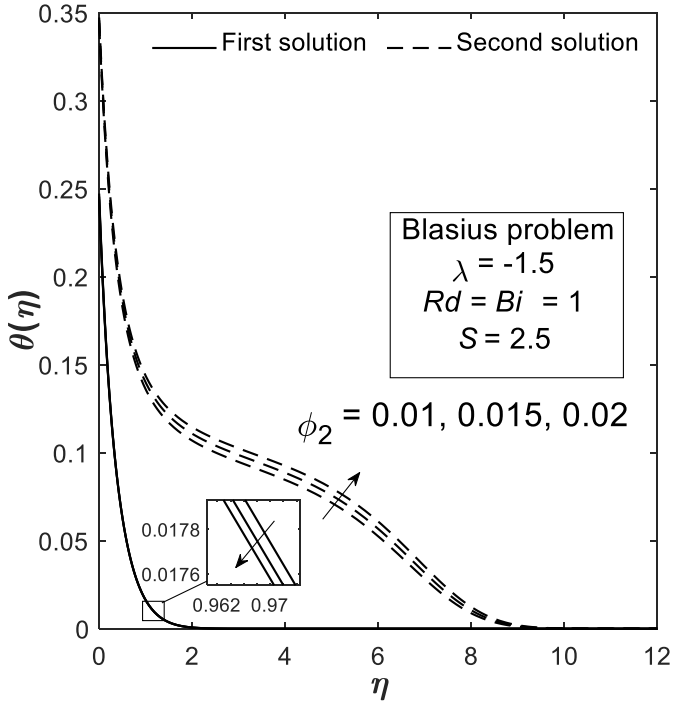

Fig. 9. Temperature profile for selected ϕ_2

Finally, the result on the stability analysis is depicted in Figure 10 via the plots of the smallest eigenvalues with λ around the selected critical point $(\lambda_c = -2.2882)$. The smallest eigenvalues for both solutions are seen to approach zero when $\lambda \to \lambda_c$ due to the growth and decay of perturbation that finally stop at λ_c. The first solution of the smallest eigenvalues is noted to be positive, implying that there is a decay in perturbation which validates that the solution is stable. Differently, the second solution of the smallest eigenvalues is negative, implying that there is an initial development of

perturbation that causes the solution to have a non-stable property. Therefore, we should only rely on the findings from the first solution for Figure 2 to Figure 9.

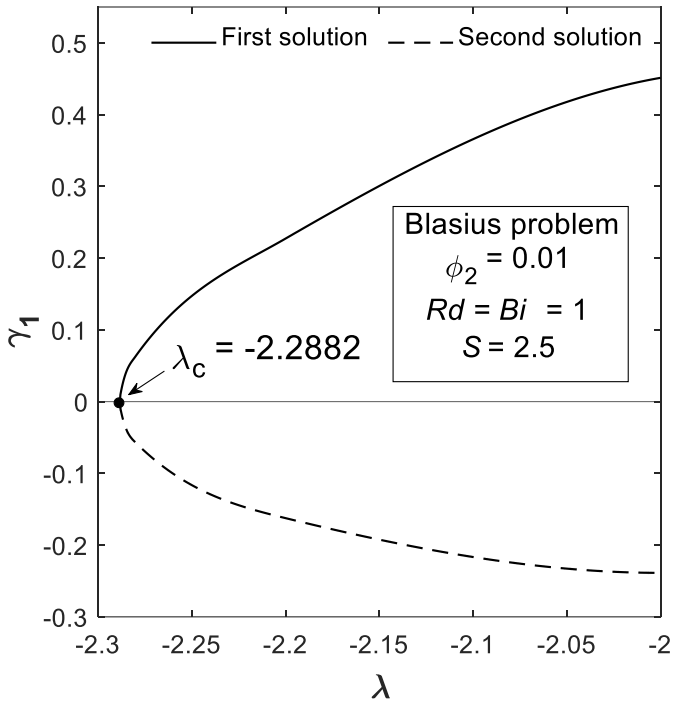

Fig. 10. Distribution of the smallest eigenvalues

6. Conclusion

The hybrid nanofluid flow with convective heated boundary, suction and thermal radiation over a permeable moving plate has been successfully envisaged for the case of Blasius model. The ordinary differential equations that govern the flow model are obtainable with the transformation of similarity from the partial differential equations. A solver in Matlab known as bvp4c is used to compute the numerical solutions. Dual solutions are generated for the condition when the plate is moving as opposed to the flow (plate moving towards the slit). The stability analysis has verified that only the first solution is stable. Thus, the following key findings are according to the reliable first solution

i. The heat transfer is improvable by enlarging the suction effect, Biot number and the thermal radiation effect, with a lesser volume fraction of copper at both (oppose or assist the flow) directions of the moving plate.
ii. In the absence of suction, a higher copper volume fraction in the alumina-water nanofluid could improve the heat transfer rate but the opposite observation is noticed during the presence of stronger suction.
iii. When the plate is moving in opposition to the flow direction, higher skin friction is obtainable by considering a higher volume fraction of copper, and vice versa when the plate is moving in a similar direction as the flow.
iv. By configuring 2% copper volume fraction, the boundary layer separation can be better prevented compared to 1% copper volume fraction.
v. Stronger suction with the amount of 2.7 causes the boundary layer separation process to be further delayed compared to 2.5 suction amount.

vi. The configuration of different values of Biot number and thermal radiation parameter are affectless towards the process of the boundary layer separation.

These findings are solely based on the present flow problem and are only valid for the hybridization of 1% volume fraction of alumina with 1-2% volume fraction of copper. Different parameters configuration might give different findings compared to the present study. The Blasius flow model can be further extended towards a ternary hybrid nanofluid with other base fluids like ethylene glycol, and with other types of nanoparticles.

Acknowledgement
The authors acknowledge the financial support from Universiti Putra Malaysia [GP-GPB 9711400].

References

[1] Blasius, Heinrich. *Grenzschichten in Flüssigkeiten mit kleiner Reibung*. Druck von BG Teubner, 1907.
[2] Sakiadis, B. C. "Boundary layer behavior on continuous solid surface; The boundary layer on a continuous moving surface." *AIChE Journa*l 7, no. 1 (1961): 26-28. https://doi.org/10.1002/aic.690070108
[3] Sakiadis, B. C. "Boundary-layer behavior on continuous solid surfaces: II. The boundary layer on a continuous flat surface." *AIChE Journal* 7, no. 2 (1961): 221-225. https://doi.org/10.1002/aic.690070211
[4] Bataller, Rafael Cortell. "Radiation effects in the Blasius flow." *Applied Mathematics and Computation* 198, no. 1 (2008): 333-338. https://doi.org/10.1016/j.amc.2007.08.037
[5] Bataller, Rafael Cortell. "Radiation effects for the Blasius and Sakiadis flows with a convective surface boundary condition." *Applied Mathematics and Computation* 206, no. 2 (2008): 832-840. https://doi.org/10.1016/j.amc.2008.10.001
[6] Aziz, Abdul. "A similarity solution for laminar thermal boundary layer over a flat plate with a convective surface boundary condition." *Communications in Nonlinear Science and Numerical Simulation* 14, no. 4 (2009): 1064-1068. https://doi.org/10.1016/j.cnsns.2008.05.003
[7] Ishak, Anuar, Nor Azizah Yacob, and Norfifah Bachok. "Radiation effects on the thermal boundary layer flow over a moving plate with convective boundary condition." *Meccanica* 46, no. 4 (2011): 795-801. https://doi.org/10.1007/s11012-010-9338-4
[8] Ahmad, Syakila, Azizah Mohd Rohni, and Ioan Pop. "Blasius and Sakiadis problems in nanofluids." *Acta Mechanica* 218, no. 3 (2011): 195-204. https://doi.org/10.1007/s00707-010-0414-6
[9] Bachok, Norfifah, Anuar Ishak, and Ioan Pop. "Flow and heat transfer characteristics on a moving plate in a nanofluid." *International Journal of Heat and Mass Transfer* 55, no. 4 (2012): 642-648. https://doi.org/10.1016/j.ijheatmasstransfer.2011.10.047
[10] Choi, S. US, and Jeffrey A. Eastman. *Enhancing thermal conductivity of fluids with nanoparticles*. No. ANL/MSD/CP-84938; CONF-951135-29. Argonne National Lab.(ANL), Argonne, IL (United States), 1995.
[11] Sarkar, Jahar, Pradyumna Ghosh, and Arjumand Adil. "A review on hybrid nanofluids: recent research, development and applications." *Renewable and Sustainable Energy Reviews* 43 (2015): 164-177. https://doi.org/10.1016/j.rser.2014.11.023
[12] Sidik, Nor Azwadi Che, Muhammad Mahmud Jamil, Wan Mohd Arif Aziz Japar, and Isa Muhammad Adamu. "A review on preparation methods, stability and applications of hybrid nanofluids." *Renewable and Sustainable Energy Reviews* 80 (2017): 1112-1122. https://doi.org/10.1016/j.rser.2017.05.221
[13] Berrehal, Hamza, Saeed Dinarvand, and Ilyas Khan. "Mass-based hybrid nanofluid model for entropy generation analysis of flow upon a convectively-warmed moving wedge." *Chinese Journal of Physics* 77 (2022): 2603-2616. https://doi.org/10.1016/j.cjph.2022.04.017
[14] Sulochana, C., and T. Prasanna Kumar. "Regression modelling of hybrid nanofluid flow past an exponentially stretching/shrinking surface with heat source-sink effect." *Materials Today: Proceedings* 54 (2022): 669-676. https://doi.org/10.1016/j.matpr.2021.10.375
[15] Sulochana, C., and T. Prasanna Kumar. "Electromagnetohydrodynamic boundary layer flow in hybrid nanofluid with thermal radiation effect: Numerical simulation." *Heat Transfer* 51, 5 (2022): 4485-4503. https://doi.org/10.1002/htj.22509
[16] Sulochana, C. and T. Prasanna Kumat. "Heat Transfer of SWCNT-MWCNT Based Hybrid Nanofluid Boundary Layer Flow with Modified Thermal Conductivity Model." *Journal of Advanced Research in Fluid Mechanics and Thermal Sciences* 92, no. 2 (2022): 13-24. https://doi.org/10.37934/arfmts.92.2.1324

[17] Dinarvand, Saeed, Seyed Mehdi Mousavi, Mohammad Yousefi, and Mohammadreza Nademi Rostami. "MHD flow of MgO-Ag/water hybrid nanofluid past a moving slim needle considering dual solutions: An applicable model for hot-wire anemometer analysis." *International Journal of Numerical Methods for Heat & Fluid Flow* 32, no. 2 (2021): 488-510. https://doi.org/10.1108/HFF-01-2021-0042

[18] Wahid, Nur Syahirah, Norihan Md Arifin, Najiyah Safwa Khashi'ie, Rusya Iryanti Yahaya, Ioan Pop, Norfifah Bachok, and Mohd Ezad Hafidz Hafidzuddin. "Three-Dimensional Radiative Flow of Hybrid Nanofluid Past a Shrinking Plate with Suction." *Journal of Advanced Research in Fluid Mechanics and Thermal Sciences* 85, no. 1 (2021): 54-70. https://doi.org/10.37934/arfmts.85.1.5470

[19] Wahid, Nur Syahirah, Norihan Md Arifin, Najiyah Safwa Khashi'ie, Ioan Pop, Norfifah Bachok, and Ezad Hafidz Hafidzuddin. "MHD hybrid nanofluid flow with convective heat transfer over a permeable stretching/shrinking surface with radiation." *International Journal of Numerical Methods for Heat & Fluid Flow* 32, no. 5 (2021): 1706-1727. https://doi.org/10.1108/HFF-04-2021-0263

[20] Wahid, Nur Syahirah, Norihan Md Arifin, Najiyah Safwa Khashi'ie, Ioan Pop, Norfifah Bachok, and Mohd Ezad Hafidz Hafidzuddin. "Unsteady mixed convective stagnation point flow of hybrid nanofluid in porous medium." *Neural Computing and Applications* 34 (2022): 14699-14715. https://doi.org/10.1007/s00521-022-07323-0

[21] Wahid, Nur Syahirah, Norihan Md Arifin, Najiyah Safwa Khashi'ie, Ioan Pop, Norfifah Bachok, and Mohd Ezad Hafidz Hafidzuddin. "Three-Dimensional Stretching/Shrinking Flow of Hybrid Nanofluid with Slips and Joule Heating." *Journal of Thermophysics and Heat Transfer* 36, no. 4 (2022): 1-10. https://doi.org/10.2514/1.T6488

[22] Wahid, Nur Syahirah, Norihan Md Arifin, Najiyah Safwa Khashi'ie, Ioan Pop, Norfifah Bachok, and Mohd Ezad Hafidz Hafidzuddin. "Unsteady MHD mixed convection flow of a hybrid nanofluid with thermal radiation and convective boundary condition." *Chinese Journal of Physics* 77 (2022): 378-392. https://doi.org/10.1016/j.cjph.2022.03.013

[23] Olatundun, Abdulyaqin Taslimah, and Oluwole Daniel Makinde. "Analysis of Blasius flow of hybrid nanofluids over a convectively heated surface." In *Defect and Diffusion Forum*, vol. 377, pp. 29-41. Trans Tech Publications Ltd, 2017. https://doi.org/10.4028/www.scientific.net/DDF.377.29

[24] Khashi'ie, Najiyah Safwa, Iskandar Waini, Anuar Ishak, and Ioan Pop. "Blasius Flow over a Permeable Moving Flat Plate Containing Cu-Al_2O_3 Hybrid Nanoparticles with Viscous Dissipation and Radiative Heat Transfer." *Mathematics* 10, no. 8 (2022): 1281. https://doi.org/10.3390/math10081281

[25] Devi, SP Anjali, and S. Suriya Uma Devi. "Numerical investigation of hydromagnetic hybrid Cu-Al_2O_3/water nanofluid flow over a permeable stretching sheet with suction." *International Journal of Nonlinear Sciences and Numerical Simulation* 17, no. 5 (2016): 249-257. https://doi.org/10.1515/ijnsns-2016-0037

[26] Waini, Iskandar, Anuar Ishak, and Ioan Pop. "Flow and heat transfer of a hybrid nanofluid past a permeable moving surface." *Chinese Journal of Physics* 66 (2020): 606-619. https://doi.org/10.1016/j.cjph.2020.04.024

[27] Takabi, Behrouz, and Saeed Salehi. "Augmentation of the heat transfer performance of a sinusoidal corrugated enclosure by employing hybrid nanofluid." *Advances in Mechanical Engineering* 6 (2014): 147059. https://doi.org/10.1155/2014/147059

[28] Dinarvand, Saeed. "Nodal/saddle stagnation-point boundary layer flow of CuO-Ag/water hybrid nanofluid: a novel hybridity model." *Microsystem Technologies* 25, no. 7 (2019): 2609-2623. https://doi.org/10.1007/s00542-019-04332-3

[29] Oztop, Hakan F., and Eiyad Abu-Nada. "Numerical study of natural convection in partially heated rectangular enclosures filled with nanofluids." *International Journal of Heat and Fluid Flow* 29, no. 5 (2008): 1326-1336. https://doi.org/10.1016/j.ijheatfluidflow.2008.04.009

[30] Izady, Mohammad, Saeed Dinarvand, Ioan Pop, and Ali J. Chamkha. "Flow of aqueous Fe_2O_3-CuO hybrid nanofluid over a permeable stretching/shrinking wedge: A development on Falkner-Skan problem." *Chinese Journal of Physics* 74 (2021): 406-420. https://doi.org/10.1016/j.cjph.2021.10.018

[31] Rosseland, Svein. *Astrophysik: Auf atomtheoretischer grundlage*. Vol. 11. Springer-Verlag, 2013.

[32] Merkin, J. H. "On dual solutions occurring in mixed convection in a porous medium." *Journal of Engineering Mathematics* 20, no. 2 (1986): 171-179. https://doi.org/10.1007/BF00042775

[33] Weidman, P. D., D. G. Kubitschek, and A. M. J. Davis. "The effect of transpiration on self-similar boundary layer flow over moving surfaces." *International Journal of Engineering Science* 44, no. 11-12 (2006): 730-737. https://doi.org/10.1016/j.ijengsci.2006.04.005

[34] Harris, S. D., D. B. Ingham, and I. Pop. "Mixed convection boundary-layer flow near the stagnation point on a vertical surface in a porous medium: Brinkman model with slip." *Transport in Porous Media* 77, no. 2 (2009): 267-285. https://doi.org/10.1007/s11242-008-9309-6

[35] Abd Rahman, Nor Hathirah, Norfifah Bachok, and Haliza Rosali. "Boundary-Layer Flow and Heat Transfer of Blasius and Sakiadis Problems in Nanofluids with Partial Slip and Thermal Convection." *CFD Letters* 11, no. 12 (2019): 53-65.